

Construction of Human Ghrelin Receptor (hGHS-R1a) Model Using a Fragmental Prediction Approach and Validation through Docking Analysis

Alessandro Pedretti, Marco Villa, Marco Pallavicini, Ermanno Valoti, and Giulio Vistoli*

Istituto di Chimica Farmaceutica, Facoltà di Farmacia, Università di Milano, Viale Abruzzi 42, I-20131 Milano, Italy

Received November 18, 2005

The objective of this study was to investigate the reliability of a fragmental approach to build a full-length model of the human ghrelin receptor (hGHS-R1a) in its open state. The soundness of the model was verified by docking the tetrapeptide Gly-Ser-Ser(*n*-octanoyl)-Phe-NH₂, which represents the ghrelin active core, and a dataset of 35 peptidomimetic GH secretagogues taken from literature. Docking results confirm the relevance of two distinct subpockets: a polar cavity bearing the key residues involved in receptor activation and an aromatic/apolar subpocket, which plays a crucial role in determining the high constitutive activity of hGHS-R1a. The docking scores of both subpockets are in remarkable agreement with biological data, emphasizing that the model can be used to predict the activity of novel ligands. Moreover, the subpocket selectivity of peptidomimetic GHSs suggests a cooperative role of the aromatic/apolar subpocket. Taken globally, the results highlight the potential of the fragmental approach to build improved models for any GPCR.

Introduction

The recently discovered hormone, ghrelin, has been recognized as an important regulator of growth hormone (GH) secretion and energy homeostasis due to its orexigenic and adipogenic effects.^{1,2} The discovery of ghrelin is a classical example of reverse pharmacology: first, synthetic GH secretagogues (GHSs) were discovered (Bowers et al., 1980³), then, the GHS receptor (GHS-R) was identified and cloned (Howard et al., 1996⁴), and finally, an acylated 28-residue peptide⁵ (ghrelin peptide) was recognized as an endogenous bioactive ligand for the GHS-R (Kojima et al., 1999⁶).

Ghrelin is the first natural peptide with the hydroxy group of a serine residue (Ser3) acylated by *n*-octanoic acid, and this posttranslational modification is essential for its bioactivity.⁷ Ghrelin is produced in the stomach (in the oxyntic glands), intestine, placenta, heart, testis, kidney, pituitary, and hypothalamus, having both endocrine and paracrine effects.⁸ The concentration of circulating ghrelin is influenced by acute and chronic changes in the nutritional state.^{9,10} Ghrelin has been shown to affect a number of different systems, mainly including GH, adrenocorticotrophic hormone (ACTH), and prolactin release, feeding, gastric secretion and mobility, metabolism, cardiac performances, and cell proliferation.¹¹ Therefore, peptidomimetic GH secretagogues¹² find therapeutic applications in several pathological conditions, namely, GH deficiency, negative energy balance status, obesity, diabetes mellitus and insulin resistance, Prader-Willi syndrome, cachexia, hyperthyroidism, and hypertension.^{13,14}

The human ghrelin receptor (hGHS-R) is a member of the GPCR family, whose activation leads to generation of inositol trisphosphate (IP₃) and Ca²⁺ release through the activation of the G protein subunit Gα11.¹⁵ The GHS-R belongs to a small family of receptors for peptide hormones and neuropeptides within class I GPCRs.¹⁶ Its closest relative is the neurotensin receptor, with about 34% of protein sequence identity.¹⁷ Two different splice forms of the human GHS-R are known, namely,

hGHS-R1a and hGHS-R1b. hGHS-R1a contains 366 amino acids with seven transmembrane domains, while it is not clear if the hGHS-R1b gene is transcribed to protein *in vivo*, but theoretically, it would code for 289 amino acids with five transmembrane domains. However, hGHS-R1b does not have biological activity *in vivo*.¹⁸

Mutagenesis studies on hGHS-R1a revealed the major role of Glu-124¹⁹ in the third transmembrane helix (TM3), which, presumably, forms a salt bridge with a ligand ammonium head. Other key residues are present in TM2 (Glu-99), TM3 (Gln120 and Ser-123), and TM5 (Met213).²⁰ One of the most important features of hGHS-R1a is its constitutive activity because it is able to change into an active conformation without the presence of the agonist, signaling with about 50% of maximal activity.²¹ Mutagenesis analyses evidenced that the constitutive activity is mainly due to an aromatic cluster formed by residues in TM5 (e.g., Phe220, Phe222, and Phe226) and TM6 (e.g., Phe279, Arg283, and Phe286) that even without ligand approach the inner face of TM2 and TM3 shifting into a constitutively active form.¹⁷ In light of these findings, the binding cavity of hGHS-R1a can be considered to be formed by two subpockets: a polar cavity lined by TM2 and TM3 and a second aromatic cavity, lined by TM5 and TM6. Moreover, it is possible to consider two hGHS-R1a states: an open state, in which the two subpockets form two distinct binding sites and a close state, in which the aromatic cluster approaches the polar subpocket, and Glu124 (TM3) interacts with Arg283 (TM6).²¹ Interestingly, mutagenesis experiments on Arg283 (TM6) indicated that its mutation eliminates both agonist stimulation and constitutive activity, suggesting the implication of such a residue in the receptor activation and maybe in the interaction with the agonists. This is in agreement with biophysical studies suggesting that the activation of many GPCRs involves an inward movement of TM6 and TM7 toward TM3.²²

The open state may be involved in agonist recognition because in the constitutively active close state, the polar binding site is partially occupied by aromatic cluster residues, and Glu124 is less available for ligand interaction. Therefore, a full-length homology model of hGHS-R1a in its open state is

* To whom correspondence should be addressed. Tel: +39 02 50317545. Fax: +39 02 50317565. E-mail: giulio.vistoli@unimi.it.

generated here, and an objective of this study is to investigate peptidomimetic GH secretagogues with which subpocket preferentially interacts.

The availability of the experimental crystal structure of bovine rhodopsin has strongly supported the homology modeling of full-length G-protein-coupled receptors,²³ and in recent years, several reliable GPCR homology models appeared in the literature,²⁴ showing that they can be successfully used for virtual screening and ligand optimization.²⁵ However, the rhodopsin-based homology models have two main drawbacks: (a) because the rhodopsin crystal structure is in its inactive closed form, the obtained binding sites are often too narrow to accommodate large ligands; (b) despite a clear homology among GPCRs, the systematic use of the rhodopsin as a template can lead to rhodopsin clones, which lose their structural peculiarity to forcedly comply with rhodopsin structure. Hence, it comes as no surprise that some rhodopsin-independent methods have been proposed in the last few years. For example, the *ab initio* approaches are mainly based on physicochemical properties of the membrane environment and require the protein sequence as unique input (e.g., the Predict approach²⁶).

In general, a recent trend in folding prediction is to favor the local homology, combining more predictive algorithms²⁷ (the so-called meta prediction, as implemented in the Shotgun technology²⁸). In principle, these approaches (1) divide the amino acid sequence in fragments, (2) predict the folding of each fragment using different methods, (3) exhaustively combine the predicted fragments, obtaining several models, and (4) select the best model using suitable score functions. The GPCR modeling well suits this fragmental strategy because (1) the amino acid sequence is clearly divisible in 15 structural fragments (namely, 7 transmembrane helices, 6 loops, and 2 terminal segments), (2) fragment prediction is not really blind, but it is well known that transmembrane segments assume helix conformations, and the loops must have a global U shape in which the loop ends are close enough to join the adjacent TM segments, and (3) the rhodopsin crystal structure can still be exploited as a template to drive the final assembly of predicted fragments.

The objective of this study is to exploit the fragmental prediction strategy to build a full-length model of hGHS-R1a in its open state. First, the reliability of the model was checked by docking the tetrapeptide Gly-Ser-Ser(*n*-octanoyl)-Phe-NH₂ (EC₅₀ = 72 nM), which constitutes the active core required for agonist potency at hGHS-R1a.²⁹ In a second phase, the GHS-R1a model was extensively verified by docking a heterogeneous set of 35 peptidomimetic agonists, taken from literature, and analyzing its ability to rationalize and predict the ligand activity. As previously mentioned, the role of subpocket selectivity was also examined using the same docking calculations.

Results and Discussion

Analysis of the GHS-R1a Model. Figure 1 presents the structure of the obtained hGHS-R1a model, colored by segment, showing the typical folding of GPCR with seven transmembrane helices (the precise subdivision in segments is described in Table 3). The *N*-terminal domain (NT) mainly assumes a β -hairpin structure, involving residues between Met1 and Asp32. It is stabilized by both a network of H bonds and an electrostatic interaction between Asp32 and ammonium terminal group, which closes the hairpin motif.

The transmembrane portion (TM1–7) assumes a round calyx shape, because the extracellular side is more open than the intracellular one. This particular shape is mainly due to a set of



Figure 1. Tube structure of the GHS-R1a model colored by segment. Color legend: NT = white, TM1 = red, CL1 = green, TM2 = azure, EL1 = yellow, TM3, dark red, CL2 = violet, TM4 = pink, EL2 = indigo, TM5 = gray, CL3 = orange, TM6 = dark green, EL3 = dark yellow, TM7 = brown, CT = blue.

Table 1. Matrix of Interhelix Distances^a

helix	TM1	TM2	TM3	TM4	TM5	TM6	average distance
TM1							17.52
TM2	8.82						13.22
TM3	16.03	8.25					12.48
TM4	22.34	13.66	9.25				14.43
TM5	28.95	22.05	14.04	14.19			19.37
TM6	18.71	16.15	14.54	18.47	16.15		17.46
TM7	10.27	10.44	12.78	18.53	20.76	9.28	13.68

^aThe values, expressed in Å, are computed as described in ref 31.

proline residues in the middle of the transmembrane helices (namely, Pro97 (TM2), Pro177 (TM4), Pro224 (TM5), Pro278 (TM6), and Pro320 (TM7)) that induce typical helix bends,³⁰ enlarging the extracellular side of the transmembrane segment. The interhelix distances,³¹ as reported in Table 1, show that TM3, which bears key residues in ligand interaction, takes the most central position in the transmembrane segment, whereas TM5 takes the most peripheral one. The average interhelix distances also suggest that TM2, TM3, TM4, and TM7 compose the core of the transmembrane segment, whereas TM1, TM5, and TM6 are in a more external position.

Furthermore, the analysis of interhelix distances also allows us to shed light on the key differences between the hGHS-R1a model in its open state and bovine rhodopsin (at least with respect to the transmembrane bundle). As a rule, the interhelix distances calculated for bovine rhodopsin (as computed considering the 1F88 pdb structure, data not shown) are always shorter than those of the hGHS-R1a model. In particular, TM1, TM2, and TM4 of bovine rhodopsin give averaged distances

Table 2. Docking Scores for Both Subpockets for All Ligands in the Dataset

compound	pEC ₅₀	FlexScore _{pol}	FlexScore _{aro}	%Pose _{aro}
1	8.87	-39.01	0.00	0.0
2	9.22	-36.71	-28.48	50.0
3	7.85	-25.40	0.00	0.0
4	8.25	-30.08	-20.60	46.7
5	8.68	-33.46	-32.09	50.0
6	8.00	-26.67	0.00	0.0
7	8.32	-28.72	0.00	0.0
8	8.60	-32.96	0.00	0.0
9	8.96	-39.13	-19.16	23.3
10	8.57	-37.48	-18.70	63.3
11	7.78	-29.74	0.00	0.0
12	8.00	-32.55	0.00	0.0
13	8.07	-33.49	0.00	0.0
14	8.30	-36.74	0.00	0.0
15	8.07	-33.81	-15.75	73.3
16	7.66	-25.33	-15.21	3.3
17	7.24	-22.83	0.00	0.0
18	8.22	-33.34	0.00	0.0
19	8.52	-31.30	-15.26	16.7
20	8.40	-33.60	-19.56	10.0
21	8.52	-36.77	0.00	0.0
22	8.52	-37.01	0.00	16.7
23	8.12	-31.80	-19.94	10.0
24	9.10	-36.40	-30.32	73.3
25	8.52	-33.54	-31.73	83.3
26	8.30	-29.02	-20.34	23.3
27	7.74	-24.38	0.00	0.0
28	8.30	-30.66	-24.24	70.0
29	8.30	-28.01	-26.66	66.7
30	8.52	-35.57	-24.76	3.3
31	8.80	-32.32	-29.68	76.7
32	9.10	-35.95	-29.82	16.7
33	9.00	-39.11	0.00	0.0
34	8.22	-36.21	0.00	0.0
35	8.70	-44.79	0.00	0.0

^a The docking scores, expressed in kcal/mol, involve the polar subpocket, FlexScore_{pol}, the apolar/aromatic subpocket, FlexScore_{aro}. The percentage of docking poses interacting with the apolar/aromatic subpocket is also reported (% Pose_{aro}).

very similar to those of hGHS-R1a model, whereas TM3, TM5, TM6, and TM7 give markedly shorter distances in rhodopsin than in the hGHS-R1a model. It confirms that the rhodopsin structure could not be used to model hGHS-R1a in its open space. It also suggests that the obtained model differs from the already reported hGHS-R1a model,^{17,32} which is based on rhodopsin structure and seems unsuitable to investigate hGHS-R1a in its open state.

The transmembrane segment is mainly stabilized by a set of hydrophobic interactions that involve both aromatic (e.g., the above-mentioned aromatic cluster) and aliphatic residues. The polar interactions between transmembrane helices are much rarer, but they play pivotal roles in stabilizing transmembrane folding. Among these, it is worth citing the following polar contacts: Thr64 (TM1) with Asp89 (TM2), Ser88 (TM2) with Thr133 (TM3), Asp99 (TM2) with Ser125 (TM3), Ser135 (TM3) with Ser174 (TM4), Tyr81 (TM2) with Asn324 (TM7), and Thr130 (TM3) with Tyr313 (TM7). In particular, the interaction between Asp99 (TM2) and Ser125 (TM3) seems to play a key role (as suggested by mutagenesis experiments) because it stabilizes the correct orientation of Asp124 (TM3) for ligand interaction. The polar interactions are more abundant in the intracellular side, where they approach the helices, than in the extracellular side, where they stabilize the correct conformation of the binding site.

The extracellular loops (EL1, EL2, and EL3) assume hairpin geometries stabilized by a set of H bonds and ion-pair interactions (for example, Glu202 with Arg206 in EL2 or

Lys288 with Glu296 in EL3). EL2 takes a central position, but the extracellular loops are so close that EL1 can also interact with EL3. In particular, EL1 and EL2 mainly interact through an ionic cluster, which involves Arg102 (EL1), Asp113 (EL1), Lys117 (EL1), Asp191 (EL2), and Asp194 (EL2), whereas EL3 interacts with EL1 and EL2 mainly through H bonds. As described later in the docking results, EL2 partially penetrates the transmembrane segment, forming the upper side of the polar binding site, and several residues (e.g., Asn188, Thr190, Pro192, Trp193, Arg199, Pro200, Ala204, and Val205) are involved in ligand interaction.

The cytoplasmic loops (CL1, CL2, and CL3) assume more constrained turn geometries mainly stabilized by H-bond interactions. The interactions between the cytoplasmic loops are rarer than that between extracellular loops, and the ionized residues (especially, positively charged residues) are probably involved in the interaction with both G protein and the phospholipidic heads. In general, the interactions between loops (both extracellular and intracellular) and transmembrane helices are very scarce, mainly because of the shortness of the loops, which impedes their approach to the transmembrane segment (except for EL2).

Finally, the C-terminal fragment (CT) assumes a helix-turn-helix motif. Indeed, it begins with an eighth helix (Ser327-Pro342), which is perpendicular to the seventh helix and rich in positively charged residues (e.g., Lys328, Lys329, Arg331, and Arg336) to anchor the CT to the phospholipidic heads,³³ and ends with a ninth helix (Lys347-Thr360) that is parallel to the eighth one. The helix-turn-helix motif is stabilized by a network of H bonds and some polar interactions (e.g., Lys347 with Glu354 and Arg357 with Glu361).

Docking Results on the hGHS-R1a Model. Tetrapeptide Results. Figure 2 shows the complex obtained between the ghrelin active core (Gly-Ser-Ser(*n*-octanoyl)-Phe-NH₂) and the polar subpocket of hGHS-R1a. The docking results evidence the main interactions stabilizing the complex. As confirmed by mutagenesis, the terminal ammonium group forms a salt bridge with Asp124 (TM3). The electrostatic interaction is further stabilized by charge-transfer interactions with Tyr128 (TM3) and Phe179 (TM4). The aromatic ring of the ligand's phenylalanine simultaneously realizes π - π interactions with Phe119 (TM3) and charge-transfer interactions with Arg-199 (EL2), and the unacylated serine forms an H bond with Ser123 (TM3). The terminal amide group interacts with Gln120 (TM3; the residue is not shown in Figure 2), whereas the ligand's ester function realizes H bonds with the backbone atoms of Asn188 (EL2) and Thr190 (EL2). These interactions confirm that EL2 penetrates the transmembrane segment taking part in ligand interactions through H bonds, as seen in other GPCRs.^{34,35} The octanoyl chain was accommodated in an apolar pocket, mainly lined by EL2, and it is engaged in several hydrophobic interactions, which are not displayed in Figure 2 for clarity (with side chains of Pro192, Trp193, Pro200, Ala204, and Val205).

It is interesting to observe that the main interactions of the tetrapeptide only involve residues in TM3 and EL2. On the one hand, it can justify the modest activity of this ligand (EC₅₀ = 72 nM). On the other hand, it confirms that TM3 and EL2 bear the key residues involved in ligand recognition. When analyzing all 30 computed poses for the tetrapeptide, one can observe that all solutions interact with the polar binding site and that the tetrapeptide never binds the apolar/aromatic subpocket.

Globally, these results allow us to form two preliminary objectives: (1) to verify the reliability of the hGHS-R1a model, at least with respect to the polar binding site and (2) to derive

Table 3. Definition of HGHS-R1A Segments and the Description of Templates Used in Fragmental Prediction

segment	position	length	template pdb code ^a	template description
N-T	Met1-Leu42	42	1cee (NMR)	Cdc42 with the GTPase binding domain of wasps
TM1	Leu43-Val68	26	1r7d (NMR)	membrane anchor domain of the N5a protein of the HCV virus
CL1	Ser69-Asn79	11	1f88 (2.8Å)	rhodopsine
TM2	Leu80-Val101	22	1UV7 (1.7Å)	periplasmic domain of Epsm from <i>Vibrio cholerae</i>
EL1	Arg102-Lys117	16	1gzt (1.3Å)	<i>Pseudomonas aeruginosa</i> lectin II with fucose
TM3	Leu118-Val139	22	1t6o (2.0Å)	nucleocapsid-binding domain of measles virus P protein
CL2	Glu140-Arg159	20	1tgg (2.0Å)	Rh3 designed right-handed coiled coil trimer
TM4	Val160-Val182	23	1fi0 (NMR)	Hiv-1 Vpr (13–33) peptide in micells
EL2	Gly183-Thr211	29	1i25 (NMR)	huwentoxin-II
TM5	Val212-Ile235	24	1onv (NMR)	Tfiif subunit Rap74 with Rnap II Ctd phosphatase Fcp1
CL3	Gly236-Lys263	28	1kd0 (1.9Å)	methylaspartate ammonia-lyase
TM6	Met264-Phe286	23	1f88 (2.8Å)	rhodopsine
EL3	Ser287-Asn305	19	1ej6 (3.6Å)	reovirus core
TM7	Leu306-Met326	21	1onv (NMR)	Tfiif subunit Rap74 with Rnap II Ctd phosphatase Fcp1
C-T	Ser327-Thr366	40	1i26 (NMR)	ptu-1, toxin from the assassin bug <i>Peirates turpis</i>

^a All template structures used are included in the HOMSTRAD database. The resolutions of the template crystal structures are reported in parentheses.

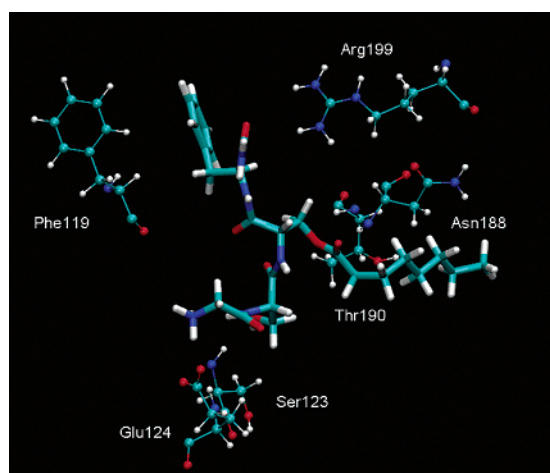
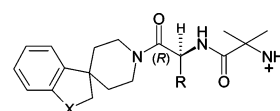


Figure 2. Three-dimensional representation of the complex realized by the tetrapeptide (Gly-Ser-Ser(*n*-octanoyl)-Phe-NH₂) in the polar subpocket of hGHS-R1a. The main interactions involve: (1) the ligand ammonium head with Asp124, (2) unacylated serine with Ser123, (3) the ligand phenyl ring with Phe119 and Arg199, and (4) the ester group with the backbone of Asn188 and Thr190.

a significant interaction pattern that will be used as a reference to evaluate the following results.

Dataset Results. The analysis of the most numerous series in the dataset (namely, the spiroindane derivatives, **1–18**, Chart 1⁴⁸) allows us to derive robust structure–activity relationships by determining the specific role of each functional group in complex stability and, hence, in the ligand's activity. Figure 3A shows a 2D scheme reporting the main interactions realized by the most active spiroindane derivative (**2**, EC₅₀ = 0.6 nM) with the polar subpocket of the hGHS-R1a model. In particular, (1) the protonated group forms an ion pair with Glu124 (TM3); (2) the indole moiety replaces tetrapeptide phenylalanine, interacting with Phe119 (TM3) and Arg199 (EL2); (3) the amidic functions replace serine residues stabilizing H bonds with Ser123 (TM3), Asn188 (EL2), and Thr190 (EL2); and (4) the spiroindane moiety mimics the octanoyl chain, realizing several hydrophobic interactions with apolar EL2 residues. What is more, the aromatic ring of spiroindane moiety interacts with Tyr106 (EL1) and Arg107 (EL1) through π – π and charge-transfer interactions, respectively, and the same residues form H bonds with the hydroxy group. When comparing **2**, **3**, and **4**, it is possible to determine the role of H bonding with Tyr106 and Arg107 on the activity of these compounds, observing that it can give a 23-fold increase of activity (0.6 nM (**2**) vs 14 nM

Chart 1. Spiroindane Derivatives⁴⁸

Compound	R	X	EC ₅₀ (nM)	Compound	R	X	EC ₅₀ (nM)
1		NSO ₂ CH ₃	1.3	10		O	2.7
2		(<i>R</i>)CHOH	0.6	11		CH ₂	17.0
3		CH ₂	14.0	12		S	10.0
4		S	5.6	13		SO	8.5
5		SO ₂	2.1	14		SO ₂	5.0
6		CH ₂	10.0	15		O	8.5
7		S	4.8	16		CH ₂	22.0
8		SO	2.0	17		S	57.0
9		SO ₂	1.1	18		SO ₂	6.0

(**3**). Similarly, comparing **5**, **9**, **14**, and **18** it is possible to shed light on the role of interactions with Phe119 and Arg199: a significant increase of activity is obtained with enlarged planar systems (as seen in the indole derivative, **5**), whereas the insertion of an oxygen atom in the alkyl bridge is detrimental for the activity (as seen in **14**), maybe because it hampers the correct orientation of the aromatic moiety without adding new specific interactions.

Taken globally, the docking results for spiroindane derivatives emphasize that the polar binding cavity of the hGHS-R1a model possesses quite a symmetrical architecture showing a central strong polar region that forms both ion pair (between the ammonium group and Asp123) and H bonds interactions (involving Ser123, Asn188, and Thr190) and two lateral hydrophobic/aromatic regions. The first hydrophobic/aromatic region, defined by Phe119, Phe121, and Arg199, is more constrained (the distance between Phe119 and Arg199 is less than 10 Å) and seems to preferentially accommodate aromatic planar moieties (e.g., the phenylalanine in tetrapeptide or the indole in **2**). The latter, lined by Tyr106, Arg107, Pro192, Trp193, Pro200, Ala204, and Val205, is ampler, accepting both aromatic (the phenyl ring of the spiroindane group) and aliphatic (the octanoyl chain in the tetrapeptide) moieties.

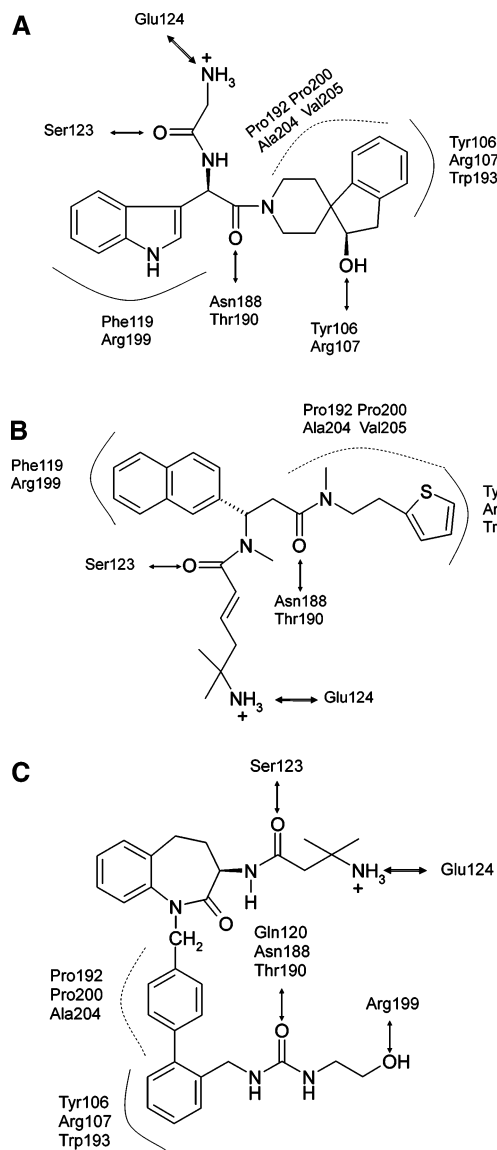
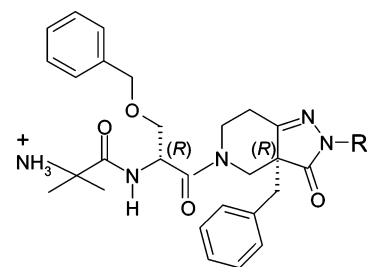


Figure 3. Two-dimensional scheme showing the main interactions realized by some significant ligands of the dataset with the polar subpocket. (A) Interaction realized by **2** ($EC_{50} = 0.6$ nM); (B) interaction realized by **24** ($EC_{50} = 0.8$ nM); and (C) interaction realized by **35** ($EC_{50} = 2.0$ nM). Figure Legend: dashed line = hydrophobic contacts; line = charge transfer and π - π interactions; bold arrow = ion interactions; arrow = H-bond interactions.

Although a systematic analysis of all ligands in the dataset has been avoided, some complexes deserve the reader's attention. For example, Figure 3B shows the remarkable pattern of interactions afforded by the most active α,β -unsaturated derivative (**24**, $EC_{50} = 0.8$ nM, Chart 3). It partially breaks the interaction symmetry, as seen in spiroindane derivatives, showing that strong interactions with Phe119 and Arg199 can somewhat counteract those with Tyr106 and Arg107. Indeed, its naphthyl group is tightly inserted between Phe119 and Arg199, whereas the thiophenyl moiety weakly interacts with Tyr106 and Arg107 without forming significant H bonds.

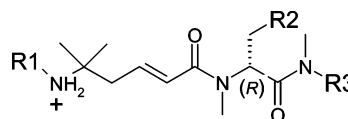
Figure 3C reports the main interactions realized by benzolactam derivative **35** ($EC_{50} = 2.0$ nM, Chart 5), showing a markedly different pattern. Indeed, it conserves the hydrophobic interactions of the diphenyl moiety that mimics the octanoyl chain, but it is lacking in the second aromatic portion because the benzolactam moiety is too close to the ammonium head to interact with Phe119 and Arg199. Finally, the aminocarbonyl-

Chart 2. Pyrazolinone-Piperidine Derivatives⁴⁹



Compound	R	EC_{50} (nM)
19	CH ₃	3.0
20	CH ₂ CH ₃	4.0
21	H	3.0

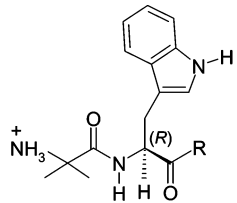
Chart 3. α,β -Unsaturated Derivatives⁵⁰



Compound	R1	R2	R3	EC_{50} (nM)
22	H			3.0
23	H			7.5
24	CH ₃			0.8
25	CH ₃			3.0
26	H			5.0
27	H			18.0
28	H			5.0
29	CH ₃			5.0

amino substituent mimics the serine residues in the tetrapeptide, forming H bonds with Gln120, Asn188, and Thr190, and the terminal hydroxy function interacts with Arg199. The relevance of this unusual interaction (normally, Arg199 interacts with aromatic moieties) can be confirmed by the lower activity of **34** ($EC_{50} = 6.0$ nM).

Taken globally, the docking results confirm the role of three hot regions in the polar subpocket: the central polar area, where the ion pair between the ligand ammonium group and Glu124 seems mandatory for the ligand activity and two lateral hydrophobic/aromatic areas, where both apolar and polar interactions are possible. Clearly, the most active compounds suitably interact with all three hot areas (as seen in Figure 3A), but the obtained results may demonstrate that strong interactions

Chart 4. Indol Derivatives⁵¹


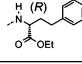
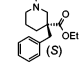
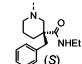
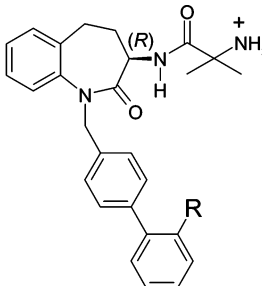
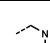
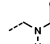
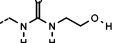
Compound	R	EC ₅₀ (nM)
30		3.0
31		1.6
32		0.8

Chart 5. Benzolactam Derivatives⁵²


Compound	R	EC ₅₀ (nM)
33		1.0
34		6.0
35		2.0

with an apolar area can counterbalance weak or partial interactions with the other apolar region (as seen in Figure 3B and C).

As examined later in the next section, the best score poses for all ligands within the dataset involve the polar subpocket. Figure 4A reports the relationship between activity values (expressed as pEC₅₀) and best score values (as compiled in Table 2, FlexScore_{pol} values), showing a significant agreement between their trends. The soundness of this relationship is markedly confirmed by statistical parameters, calculated by QSAR software³⁶ (as seen in eq 1), suggesting that these docking analyses can be successfully used to predict the ligand's activity.

$$\text{pEC}_{50} = 6.06 (\pm 0.35) - 0.070 (\pm 0.01) \text{FlexScore}_{\text{pol}} \quad (1)$$

$$n = 35; r^2 = 0.57; q^2 = 0.51; s = 0.29; F = 44.30$$

Clearly, the statistical parameters can be further improved, considering homogeneous ligand sets (for example, the spiroindane derivatives alone give a relationship with $r^2 = 0.69$ and $n = 18$), but the soundness of this model lies in its ability to also predict biological activities for heterogeneous datasets.

Although the statistical parameters could be fortuitously overvalued by some approximations of docking simulations (i.e., the rigidity of protein structure, overestimation of polar contacts, and the suitability of the score function), the obtained results

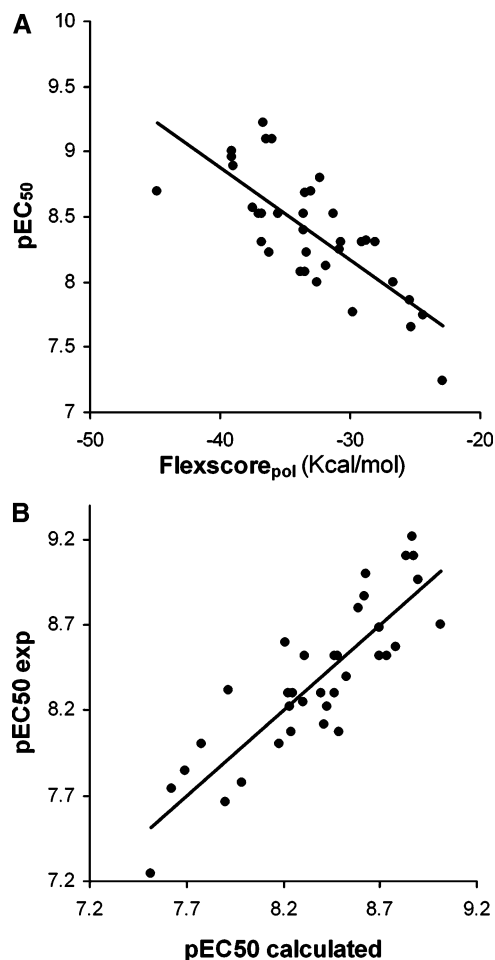


Figure 4. Correlations between biological activities (expressed as pEC₅₀) and docking scores. (A) Correlation obtained considering the best scores for the polar subpocket of the hGHS-R1a model. (FlexScore_{pol}, in kcal/mol) (B) correlation obtained considering the best scores for both the polar and aromatic subpockets of the hGHS-R1a model.

seem to afford an encouraging validation of the hGHS-R1a homology model, confirming the reliability of fragmental prediction approaches to derive improved full-length models of GPCRs.

Subpocket Selectivity. As described in the Introduction section, the open GHS-R1a model has two distinct subpockets: a polar one, whose interaction capacity was carefully examined in a previous section and a second apolar/aromatic subpocket defined by the inner face of TM6 and TM7. The subpockets are so distant that a ligand cannot simultaneously interact with both, and the docking conditions are appositely chosen to include both subpockets and to analyze the peptidomimetic GH secretagogues with which they preferentially interact.

The docking results of previous sections demonstrated that the best pose for all considered ligands always involve the polar binding site. This subpocket selectivity is understandable because the polar cavity includes all key residues involved in receptor activation. On the basis of these findings, the questions are (1) whether the ligands can also interact with the second apolar/aromatic subpocket and (2) whether this interaction can somewhat contribute to ligand activity.

To answer to the first question, all 30 poses computed for each ligand in the dataset were examined, finding at least one pose, which interacts with the apolar/aromatic subpocket, in 18 out of 35 considered ligands (as seen in Table 2), and in 6 cases

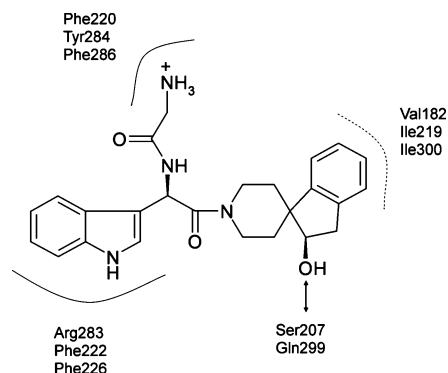


Figure 5. Two-dimensional scheme showing the main interactions realized by **2** with the apolar/aromatic subpocket. The legend is the same as that for Figure 3.

(namely, **10**, **15**, **24**, **25**, **28**, and **31**), the poses interacting with the apolar/aromatic subpocket represent a significant majority.

Figure 5 shows a 2D scheme of the main interactions realized by the most active ligand (**2**) in the apolar/aromatic subpocket. Clearly, the polar interactions are very scarce, and the main interacting moieties are afforded by hydrophobic residues. In particular, (1) the indole moiety realizes charge transfer and π - π interactions with Phe222, Phe226, and Arg283; (2) the ammonium head is involved in charge-transfer interactions with Phe220, Tyr284, and Phe286; (3) the spiroindane moiety is engaged in several hydrophobic interactions with Val131, Ile134, Val182, Ile219, and Ile300; and (4) the sole polar interactions involve the hydroxy function forming H bonds with Ser207 and Gln299. Moreover, the other ligands interacting with the apolar/aromatic subpocket give an interaction pattern very similar to that described in Figure 5 (results not shown).

To understand if the apolar/aromatic binding site can have a role in the ligand's activity, eq 1 was recalculated including the docking scores for both subpockets (as compiled in Table 2, i.e., $\text{FlexScore}_{\text{pol}}$ for the polar subpocket and $\text{FlexScore}_{\text{aro}}$ for the apolar/aromatic subpocket).

$$\text{pEC}_{50} = 5.96 (\pm 0.29) - 0.068 (\pm 0.0087) \text{FlexScore}_{\text{pol}} - 0.014 (\pm 0.0033) \text{FlexScore}_{\text{aro}} \quad (2)$$

$$n = 35; r^2 = 0.72; q^2 = 0.67; s = 0.24; F = 42.06$$

Eq 2 demonstrates that the inclusion of a second docking score ($\text{FlexScore}_{\text{aro}}$) markedly improves the statistical soundness of the correlative equation ($r^2 = 0.72$ vs $r^2 = 0.57$, as seen in Figure 4B). It may suggest that ligand interactions with the apolar/aromatic subpocket are not an artifact of docking calculations but that they can play a sensible role in receptor activation. What is more, the docking results show that the most active subnanomolar ligands (e.g., **2**, **24**, and **32**) are able to successfully interact with both subpockets, suggesting a cooperative effect of two binding modes.

This effect can be explained because the interaction with the apolar/aromatic subpocket can promote the transition of hGHS-R1a into a constitutively active state through a noncompetitive partial agonist mechanism. It means that the experimental activity can be considered as a weighted sum of a full agonism in a polar binding site and a partial agonism in an aromatic/apolar subpocket.

It is worth emphasizing that with the lack of additional experimental data the reported computational results can be only suggestive of different binding modes, and other explanations could be given to take them into account. Nonetheless, the

results appear consistent with a recent study by Holst and co-workers, who demonstrated that some peptidomimetic GHSs surprisingly act as positive allosteric modulators that increase ghrelin's potency (whereas **1** acts as a simple agonist).³⁷

Finally, the relevance of the aromatic/apolar subpocket lies in the possibility to exploit it in designing inverse agonists that bind the aromatic cluster, impeding helix movements and reducing constitutive activity. Such a behavior was already observed for some substance P analogues, and it would be useful in suppressing appetites in the treatment of obesity.²¹

Conclusions

GHS-R1a was chosen both for its crucial role in several physio-pathological processes and for its structural features that markedly differ from those of rhodopsin and most GPCRs. The major structural peculiarities of GHS-R1a concern (1) the transmembrane bundle, which is markedly wide, defining two distinct binding sites and (2) the loops, which are at the same time short and flexible. The first feature can be explained by considering the large size of the endogenous ligand, and indeed, it is common to GPCRs interacting with peptide hormones and neuropeptides. The second feature is strictly related to the high constitutive activity of GHS-R1a because short and flexible loops make possible the spontaneous movements of helices that shift GHS-R1a into a constitutively active state. Interestingly, the second feature also distinguishes GHS-R1a from many other GPCRs interacting with peptidic substrates that have short but tethered loops and show an undetectable constitutive activity (e.g., the motilin receptor which possesses rich-proline constrained loops³⁵).

On these grounds, it was clear that the open state of hGHS-R1a is quite unpredictable using rhodopsin-based approaches, but it requires a method that is able to account for local peculiarities, even ensuring a global similarity with rhodopsin folding. The proposed approach fulfils these quests because the fragmented prediction allows the exploration of local properties, whereas the final assembly ensures a substantial agreement with rhodopsin conformation.

The docking results highlight the remarkable potential of this prediction strategy to obtain improved GPCR models, especially with respect to the correct geometry of binding sites that are wide enough to accommodate any ligand without deforming the binding architecture. In principle, this approach can be applied to any GPCR member and can be exploited in mutagenesis experiments to predict local changes in the conformation of mutated GPCR proteins.

Computational Methods

Construction of GHS-R1a Starting Models. The amino acid sequence of the human GHS-R1a receptor was retrieved from Swiss-Prot database³⁸ (entry code Q92847, GHSR_HUMAN). As mentioned in the Introduction, the hGHS-R1a starting model was generated using a strategy that involves (1) the fragmentation of the amino acid sequence in 15 segments (namely, 7 TM segments, 6 loops, and 2 terminal segments), (2) the homology modeling of these segments separately, and (3) the assembly of fragments using rhodopsin structure as the template. The subdivision of the amino acid sequence was carried out using TMPRED,^{39,40} which defines the length and position of the seven transmembrane segments, as reported in Table 3.

The 15 segments were separately predicted using the Fugue approach,⁴¹ an on-line 3D structure prediction software. For each segment, Fugue is able to produce several realistic models, and the best structure has been chosen considering the result that fulfilled the following major conditions better: (a) the predicted secondary structure from the sequence alignment; (b) the lack of unpredicted

gaps; (c) the prediction score (ZSCORE) calculated by the Fugue program; (d) the helix conformation of seven transmembrane segments with the characteristic slight bend of helices containing proline and glycine residues; (e) the global U shape for the loops in which the two ends are close enough to join to adjacent TM segments; (f) the disulfide bridge between Cys126 (TM3) and Cys304 (EL2) that tethers the structure of almost all GPCRs;⁴² and (g) the presence of an eighth helix in the starting portion of the CT segment placed at a straight angle with respect to the TM7 helix.

Table 3 reports the templates used by Fugue to generate the best model for each fragment. It is interesting to observe that only two fragments (LC1 and TM6) were modeled using the rhodopsin structure as the template, whereas the other segments were built using different templates. It confirms the structural divergences between hGHS-R1a and rhodopsin and emphasizes the utility in exploring local homologies to account for them.

Finally, the assembly of predicted fragments was performed by superimposing the backbone of a fragment with that of the corresponding segment in the rhodopsin structure (pdb id: 1f88) and manually connecting the adjacent segments using the VEGA software.⁴³ In particular, the superimposition involved the C α atoms of only the transmembrane helices because the loop arrangements are clearly defined by the position of TMs, and their conformation was further relaxed by successive MD simulations (whereas the transmembrane bundle remains constrained during the molecular dynamics, as described later in the next section).

Rotamer libraries were applied to insert side chains, and hydrogen atoms were added using VEGA. According to physiological pH, the Arg, Lys, Glu, and Asp residues were preserved ionized, whereas the His residues were considered neutral by default. After a careful visual scrutiny of the obtained structure to avoid unphysical conditions, the hGHS-R1a model underwent an initial minimization until RMS = 1 to discard high-energy interactions, followed by a local minimization until RMS = 0.05, where all atoms were kept fixed except for atoms included within a 7.5 Å sphere around the manually connected bonds (at the fragment ends). Finally, the model was optimized by a final minimization made up of two phases: first, a minimization without constraints until RMS = 0.1 and then a second minimization with the backbone fixed until RMS = 0.01 to preserve the predicted structure. In these phases and in the following steps, the soundness of the model was assessed using Procheck⁴⁴ and Verify3D.⁴⁵

Model Equilibration. To gain a better relaxation and a more correct arrangement of the whole GHR-1a model, a molecular dynamics equilibration was performed in vacuo. The simulations were carried out in 3 phases: (1) heating from 0 to 300 K over 3000 iterations (3 ps, i.e., 1 K/10 iterations), (2) starting equilibration of 2500 ps, where the transmembrane backbone was kept fixed, and (3) equilibration of 7500 ps in which the transmembrane backbone was harmonically restrained with decreasing harmonic force constants. Furthermore, the harmonic force constant value was equal to 1 (1000 kJ·mol⁻¹·nm⁻²) at the beginning of simulation and then was divided into two every 1.5 ns (then 5 MD simulations were performed with the harmonic force constant equal to 1, 0.5, 0.25, 0.12, and 0.06). Globally, the MD simulation lasted 10 ns, and the helices were correctly preserved with the harmonic force constant equal to 0.06. The last frame was used for the docking calculations after a final minimization until RMS = 0.01 (with the harmonic force constant equal to 0.06).

The MD simulations had the following general characteristics: constant temperature at 300 ± 10 K by means of Langevin's algorithm; Lennard-Jones (L-J) interactions were calculated with a cutoff of 10 Å, and the pair list was updated every 20 iterations; Newton's equation was integrated using the r-RESPA method every 4 fs for long-range electrostatic forces, 2 fs for short-range non bonded forces, and 1 fs for bonded forces; a frame was stored every 5 ps, yielding 2000 frames. All calculations were carried out in a dual Athlon PC. The package Namd2.51⁴⁶ was used with the force-field CHARMM v22 and Gasteiger's atomic charges. All minimizations in model construction and equilibration were performed using the conjugated gradients algorithm.

GHS Dataset. A dataset with 35 heterogeneous peptidomimetic GH secretagogues was compiled from literature, considering GHR-1a agonists for which the biological activity was evaluated through the in vitro assay of GH release from rat pituitary cells.⁴⁷ The choice of this kind of biological data is mainly due to the following reasons: (1) a vast majority of pharmacological data reported in the literature for GHSs is obtained using this assay, which seems to be a unique, well-standardized method yielding fully comparable results; and (2) when analyzing the agonist specificity toward two distinct binding sites, the activities may be more informative than the affinity values.

For each considered series, only the most active compounds were included in the dataset (i.e., with EC₅₀ < 100 nM). According to their structure, the GHSs can be classified in five classes: spiroindanes⁴⁸ (**1–18** including MK-0677, Chart 1), pyrazolinone-piperidines⁴⁹ (**19–21** including capromorelin, Chart 2), α,β -unsaturated derivatives⁵⁰ (**22–29**, Chart 3), indoles⁵¹ (**30–32** Chart 4), and benzolactams⁵² (**33–35**, Chart 5). The biological activities within the dataset ranged from 0.6 (**2**) to 57 nM (**17**). As suggested by the pharmacophore hypothesis,⁵³ all selected GHSs possess an ionisable amine group, at least one H-bond acceptor function, and at least two aromatic moieties.

The GHSs were built preserving the stereochemistry reported in the literature (as indicated in Charts 1–5), and when more stereoisomers are described in the literature, only the most active one was considered in the docking analysis. The compounds were simulated in their protonated form because it is involved in receptor recognition. After a preliminary energy minimization to discard high-energy intramolecular interactions, the overall geometry and the atomic charges were optimized using MOPAC6.0 (keywords: AM1, PRECISE, GEO-OK, and MMOK). The tetrapeptide Gly-Ser-Ser(*n*-octanoyl)-Phe-NH₂ was built using VEGA and underwent the same minimization procedure as peptidomimetic GHSs.

Docking Analyses. The FlexX program was used to dock the compounds to the GHS-R1a binding sites. FlexX is a fast automated docking program that considers ligand conformational flexibility by an incremental fragment placing technique.⁵⁴ In this study, the docking analysis involved the full-length hGHS-R1a model considering all residues enclosed within a 20.0 Å radius sphere centered on Ile178 (TM4) so that the ligands can interact with the polar site or the aromatic cluster. For each molecule, 30 docking solutions (poses) were computed and scored.

References

- Korbonits, M.; Goldstone, A. P.; Gueorguiev, M.; Grossman, A. B. Ghrelin – a hormone with multiple functions. *Front. Neuroendocrinol.* **2004**, *25*, 27–68.
- Ghigo, E.; Broglio, F.; Arvat, E.; Maccario, M.; Papotti, M.; Cuccioli, G. Ghrelin: more than a natural GH secretagogue and/or an orexigenic factor. *Clin. Endocrinol.* **2005**, *62*, 1–17.
- Bowers, C. Y.; Momany, F.; Reynolds, G. A.; Chang, D.; Hong, A.; Chang, K. Structure-activity relationships of a synthetic pentapeptide that specifically releases growth hormone in vitro. *Endocrinology* **1980**, *106*, 663–667.
- Howard, A. D.; Feighner, S. D.; Cully, D. F.; Arena, J. P.; Liberators, P. L.; Roseblum, C. I.; Hamelin, M.; Liu, K. K.; Heavens, R.; Rigby, M. A receptor in pituitary and hypothalamus that functions in growth hormone release. *Science* **1996**, *273*, 974–977.
- The complete amino acid sequence of ghrelin is GSS(octanoyl)-FLSPEHQRVQQRKESKPKPPAKLQPR.
- Kojima, M.; Hosoda, H.; Date, Y.; Nakazato, M.; Matsuo, H.; Kangawa, K. Ghrelin is a growth-hormone-releasing acylated peptide from stomach. *Nature* **1999**, *402*, 656–660.
- Matsumoto, M.; Hosoda, H.; Morizumi, N.; Hayashi, Y. Structure-activity relationship of ghrelin: pharmacological study of ghrelin peptides. *Biochem. Biophys. Res. Commun.* **2001**, *287*, 142–146.
- Kojima, M.; Kangawa, K. Ghrelin: structure and function. *Physiol. Rev.* **2005**, *85*, 495–522.
- Otto, B.; Spranger, J.; Benoit, S. C.; Clegg, D. J.; Tschop, M. H. The many faces of ghrelin: new perspectives for nutrition research? *Br. J. Nutr.* **2005**, *93*, 765–771.
- Ueno, H.; Yamaguchi, H.; Kangawa, K.; Nakazato, M., Ghrelin: a gastric peptide that regulates food intake and energy homeostasis. *Regul. Pept.* **2005**, *126*, 11–19.

- (11) van der Lely, A. J.; Tschop, M.; Heiman, M. L.; Ghigo, E. Biological, physiological, pathophysiological, and pharmacological aspects of ghrelin. *Endocr. Rev.* **2004**, *25*, 426–457.
- (12) Smith, R. G. Development of growth hormone secretagogues. *Endocr. Rev.* **2005**, *26*, 346–360.
- (13) Cummings, D. E.; Foster-Schubert, K. E.; Overduin, Ghrelin and energy balance: focus on current controversies. *J. Curr. Drug. Targets* **2005**, *6*, 153–169.
- (14) Smith, R. G.; Sun, Y.; Betancourt, L.; Asnicar, M. Growth hormone secretagogues: prospects and potential pitfalls. *Best Pract. Res., Clin. Endocrinol. Metab.* **2004**, *18*, 333–347.
- (15) McKee, K. K.; Palyha, O. C.; Feighner, S. D.; Hreniuk, D. L.; Tan, C. P.; Phillips, M. S.; Smith, R. G.; Van der Ploeg, L. H.; Howard, A. D. Molecular analysis of rat pituitary and hypothalamic growth hormone secretagogue receptors. *Mol. Endocrinol.* **1997**, *11*, 415–423.
- (16) Smith, R. G.; Leonard, R.; Bailey, A. R. T.; Palyha, O.; Feighner, S.; Tan, C.; McKee, K. K.; Pong, S.-S.; Griffin, P.; Howard, A. Growth hormone secretagogue receptor family members and ligands. *Endocrine* **2001**, *14*, 9–14.
- (17) Holst, B.; Holliday, N. D.; Bach, A.; Elling, C. E.; Cox, H. M.; Schwartz, T. W. Common structural basis for constitutive activity of the ghrelin receptor family. *J. Biol. Chem.* **2004**, *279*, 53806–53817.
- (18) Petersenn, S.; Rasch, A. C.; Penschorn, M.; Beil, F. U.; Schulte, H. M. Genomic structure and transcriptional regulation of the human growth hormone secretagogue receptor. *Endocrinology* **2001**, *142*, 2649–2659.
- (19) In this article, the residues are progressively numbered from 1 to 366, irrespective of the corresponding segment.
- (20) Feighner, S. D.; Howard, A. D.; Prendergast, K.; Palyha, O. C.; Hreniuk, D. L.; Nargund, R.; Underwood, D.; Tata, J. R.; Dean, D. C.; Tan, C. P.; McKee, K. K.; Woods, J. W.; Patchett, A. A.; Smith, R. G.; van der Ploeg, L. H. T. Structural requirements for the activation of the human growth hormone secretagogue receptor by peptide and nonpeptide secretagogues. *Mol. Endocrinol.* **1998**, *12*, 137–145.
- (21) Holst, B.; Cygankiewicz, A.; Jensen, T. H.; Ankersen, M.; Schwartz, T. W. High constitutive signaling of the ghrelin receptor—identification of a potent inverse agonist. *Mol. Endocrinol.* **2003**, *17*, 2201–2210.
- (22) Elling, C. E.; Thirstrup, K.; Holst, B.; Schwartz, T. W. Conversion of agonist site to metal-ion chelator site in the beta(2)-adrenergic receptor. *Proc. Natl. Acad. Sci. U.S.A.* **1999**, *96*, 12322–12327.
- (23) Filipek, S.; Teller, D. C.; Palczewski, K.; Stenkamp, R. The crystallographic model of rhodopsin and its use in studies of other G protein-coupled receptors. *Annu. Rev. Biophys. Biomol. Struct.* **2003**, *32*, 375–397.
- (24) Fanelli, F.; De Benedetti, P. G. Computational modeling approaches to structure—function analysis of G protein-coupled receptors. *Chem. Rev.* **2005**, *105*, 3297–3351.
- (25) Evers, A.; Hessler, G.; Matter, H.; Klabunde, T. Virtual screening of biogenic amine-binding G-protein coupled receptors: Comparative evaluation of protein- and ligand-based virtual screening protocols. *J. Med. Chem.* **2005**, *48*, 5448–5465 and references cited herein.
- (26) Shacham, S.; Topf, M.; Avisar, N.; Glaser, F.; Marantz, Y.; Bar-Haim, S.; Noiman, S.; Naor, Z.; Becker, O. M. Modeling the 3D structure of GPCRs from sequence. *Med. Res. Rev.* **2001**, *21*, 472–483.
- (27) Ginalski, K.; Grishin, N. V.; Godzik, A.; Rychlewski, L. Practical lessons from protein structure prediction. *Nucleic Acids Res.* **2005**, *33*, 1874–1891.
- (28) Fischer, D. 3D-Shotgun: a novel cooperative fold-recognition meta-predictor. *Proteins* **2003**, *51*, 434–441.
- (29) Bednarek, M. A.; Feighner, S. D.; Pong, S. S.; McKee, K. K.; Hreniuk, D. L.; Silva, M. V.; Warren, V. A.; Howard, A. D.; van Der Ploeg, L. H.; Heck, J. V. Structure—function studies on the new growth hormone-releasing peptide, ghrelin: minimal sequence of ghrelin necessary for activation of growth hormone secretagogue receptor 1a. *J. Med. Chem.* **2000**, *43*, 4370–4376.
- (30) Riek, R. P.; Rigoutsos, I.; Novotny, J.; Graham, R. M. Nonalpha-helical elements modulate polytopic membrane protein architecture. *J. Mol. Biol.* **2001**, *306*, 349–362.
- (31) The average distance between a pair of helices was calculated by averaging the lowest distances obtained considering all possible residues of the second helix for each residue of the first helix. The position of each residue is defined only by the C α atom.
- (32) Bondensgaard, K.; Ankersen, M.; Thogersen, H.; Hansen, B. S.; Wulff, B. S.; Bywater, R. P. Recognition of privileged structures by G-protein coupled receptors. *J. Med. Chem.* **2004**, *47*, 888–899.
- (33) Sakmar, T. P.; Menon, S. T.; Marin, E. P.; Awad, E. S. Rhodopsin: insights from recent structural studies. *Annu. Rev. Biophys. Biomol. Struct.* **2002**, *31*, 443–484.
- (34) Pedretti, A.; Silva, M. E.; Villa, L.; Vistoli, G. Binding site analysis of full-length alpha(1a) adrenergic receptor using homology modeling and molecular docking. *Biochem. Biophys. Res. Commun.* **2004**, *310*, 1083–1088.
- (35) Matsuura, B.; Dong, M.; Miller, L. J. Differential determinants for peptide and nonpeptidyl ligand binding to the Motilin receptor. *J. Biol. Chem.* **2002**, *277*, 9834–9839.
- (36) <ftp://dasher.wustl.edu/pub/qsar>.
- (37) Holst, B.; Brandt, E.; Bach, A.; Heding, A.; Schwartz, T. W. Nonpeptide and peptide growth hormone secretagogues act both as ghrelin receptor agonist and as positive or negative allosteric modulators of ghrelin signaling. *Mol. Endocrinol.* **2005**, *19*, 2400–2411.
- (38) http://www.expasy.org/uniprot/GHSR_HUMAN.
- (39) http://www.ch.embnet.org/software/TMPRED_form.html.
- (40) The sequence fragmentation was also performed using other approaches (DAS, KKD, SOSUI, TMHMM, HMMTOP) obtaining results that were quite identical.
- (41) Shi, J.; Blundell, T. L.; Mizuguchi, K., FUGUE: sequence-structure homology recognition using environment-specific substitution tables and structure-dependent gap penalties. *J. Mol. Biol.* **2001**, *310*, 243–257.
- (42) Karnik, S. S.; Gogonea, C.; Patil, S.; Saad, Y.; Takezako, T. Activation of G-protein-coupled receptors: a common molecular mechanism. *Trends. Endocrinol. Metab.* **2003**, *14*, 431–437.
- (43) Pedretti, A.; Villa, L.; Vistoli, G. VEGA: a versatile program to convert, handle and visualize molecular structure on windows-based PCs. *J. Mol. Graphics Modell.* **2002**, *21*, 47–49.
- (44) Laskowski, R. A.; MacArthur, M. W.; Moss, D. S.; Thornton, J. M. PROCHECK: a program to check the stereochemical quality of protein structures. *J. Appl. Crystallogr.* **1993**, *26*, 283–291.
- (45) Bowie, J. U.; Luthy, R.; Eisenberg, D. A method to identify protein sequences that fold into a known three-dimensional structure. *Science* **1991**, *253*, 164–170.
- (46) Kalé, L.; Skeel, R.; Bhandarkar, M.; Brunner, R.; Gursoy, A.; Krawetz, N.; Phillips, J.; Shinozaki, A.; Varadarajan, K.; Schulten, K. NAMD2: Greater scalability for parallel molecular dynamics. *J. Comput. Phys.* **1999**, *151*, 283–312.
- (47) Heiman, M. L.; Nekola, M. V.; Murphy, W. A.; Lance, V. A.; Coy, D. H. An extremely sensitive in vitro model for elucidating structure-activity relationships of growth hormone-releasing factor analogues. *Endocrinology* **1985**, *116*, 410–415.
- (48) Chen, M. H.; Pollard, P. P.; Patchett, A. A.; Cheng, K.; Wei, L.; Chan, W. W.; Butler, B.; Jacks, T. M.; Smith, R. G. Synthesis and biological activities of spiroheterocyclic growth hormone secretagogues. *Bioorg. Med. Chem. Lett.* **1999**, *9*, 1261–1266.
- (49) Carpino, P. A.; Lefker, B. A.; Toler, S. M.; Pan, L. C.; Haddock, J. R.; Cook, E. R.; DiBrino, J. N.; Campeta, A. M.; DeNinno, S. L.; Chidsey-Frink, K. L.; Hada, W. A.; Inthavongsay, J.; Mangano, F. M.; Mullins, M. A.; Nickerson, D. F.; Ng, O.; Pirie, C. M.; Ragan, J. A.; Rose, C. R.; Tess, D. A.; Wright, A. S.; Yu, L.; Zawistoski, M. P.; DaSilva-Jardine, P. A.; Wilson, T. C.; Thompson, D. D. Pyrazolinone-piperidine dipeptide growth hormone secretagogues (GHSs). Discovery of capromorelin. *Bioorg. Med. Chem.* **2003**, *11*, 581–590.
- (50) Peschke, B.; Ankersen, M.; Hansen, T. K.; Hansen, B. S.; Lau, J.; Nielsen, K. K.; Raun, K. New highly potent dipeptidic growth hormone secretagogues with low molecular weight. *Eur. J. Med. Chem.* **2000**, *35*, 599–618.
- (51) Yang, L.; Morriello, G.; Patchett, A. A.; Leung, K.; Jacks, T.; Cheng, K.; Schleim, K. D.; Feeney, W.; Chan, W. W.; Chiu, S. H.; Smith, R. G., 1-[2(R)-(2-amino-2-methylpropionylamino)-3-(1H-indol-3-yl)propionyl]-3-benzylpiperidine-3(S)-carboxylic acid ethyl ester (L-163, 540): a potent, orally bioavailable, and short-duration growth hormone secretagogue. *J. Med. Chem.* **1998**, *41*, 2439–2441.
- (52) DeVita, R. J.; Bochis, R.; Frontier, A. J.; Kotliar, A.; Fisher, M. H.; Schoen, W. R.; Wyvratt, M. J.; Cheng, K.; Chan, W. W.; Butler, B.; Jacks, T. M.; Hickey, G. J.; Schleim, K. D.; Leung, K.; Chen, Z.; Chiu, S. L.; Feeney, W. P.; Cunningham, P. K.; Smith, R. G. A potent, orally bioavailable benzazepinone growth hormone secretagogue. *J. Med. Chem.* **1998**, *41*, 1716–1728.
- (53) Huang, P.; Loew, G. H.; Funamizu, H.; Mimura, M.; Ishiyama, N.; Hayashida, M.; Okuno, T.; Shimada, O.; Okuyama, A.; Ikegami, S.; Nakano, J.; Inoguchi, K. Rational design, discovery, and synthesis of a novel series of potent growth hormone secretagogues. *J. Med. Chem.* **2001**, *44*, 4082–4091.
- (54) Rarey, M.; Kramer, B.; Lengauer, T.; Klebe, G. A fast flexible docking method using an incremental construction algorithm. *J. Mol. Biol.* **1996**, *261*, 470–489.